Preprint
UCRL-JC-151219

Efficient Multi-ke V X-Ray Sources from Ti-Doped Aerogel Targets

K. B. Fournier, C. Constantin, J. Poco, M. C. Miller, C. A. Back, L. J. Sutter, J. Satcher, J. Davis, J. Grun

This article was submitted to *Laser-Generated and Other X-Ray and EUV Sources, Optics and Applications, San Diego, California, 08/03/2003 – 08/08/2003*

U.S. Department of Energy

Lawrence Livermore National Laboratory

July 18, 2003

This work was performed under the auspices of the U.S. Department of Energy by University of California, Lawrence Livermore National Laboratory under Contract W-7405-Eng-48.

Efficient multi-keV x-ray sources from Ti-doped aerogel targets

K. B. Fournier[a], C. Constantin[a], J. Poco[a], M. C. Miller[a], C. A. Back[a], L. J. Suter[a], J. Satcher[a], J. Davis[b] and J. Grun[c]

[a]Lawrence Livermore National Laboratory, 7000 East Avenue, Livermore, CA 94550 USA
[b]Alme & Associates, 6020 Richmond Highway, Alexandria, VA 22303 USA
[c]Plasma Physics Division, Naval Research Laboratory, 4555 Overlook Ave., SW, Washington DC 20375 USA

ABSTRACT

We have measured the production of $h\nu \geq 4.5$ keV x-rays from low-density Ti-doped aerogel targets at the OMEGA laser facility (University of Rochester). The targets were 2.2 mm long by 2 mm diameter beryllium cylinders filled with Ti-doped (3 atomic percent) SiO_2 foam. The doped-foam density was ≈ 3 mg/cc. Forty beams of the OMEGA laser ($\lambda = 351$ nm) illuminated the two cylindrical faces of the target with a total power that ranged from 7 to 14 TW. The laser interaction fully ionizes the target ($n_e/n_{\rm crit} \leq 0.1$), and allows the laser-bleaching wave to excite, supersonically, the high-Z emitter ions in the sample. The heating of the target was imaged with a gated (200 ps time resolution) x-ray framing camera filtered to observe > 4 keV. 2-D radiative-hydrodynamic calculations predict rapid and uniform heating over the whole target volume with minimal energy losses into hydrodynamic motion. An x-ray streak camera, also filtered to observe > 4 keV, was used to measure the rate of heat propagation in the target. Ti K-shell x-ray emission was spectrally resolved with a two-channel crystal spectrometer and recorded with a set of calibrated aluminum x-ray diodes. Back-scattered laser energy is observed to be minimal. We find between 100 - 400 J of output with $4.67 \leq h\nu \leq 5.0$ keV, predicted target performance is a factor of 2 – 3 too low in this range.

Keywords: X-ray source, Ti K-shell, Low-density foam, Lasers

1. INTRODUCTION

Maximizing the conversion efficiency (CE) of laser energy into multi-keV x-rays is a general concern to many areas of high-energy-density plasma physics.[1–4] Bright x-ray sources are needed for backlighters in order to radiograph targets in inertial-confinement fusion experiments.[3,4] As the targets get larger, and as compression in the targets increases, the backlighter sources need to be brighter and the backlighter photon energies must get higher. To this end, for a given laser power, backlighters can become brighter by becoming more efficient at converting the drive beams to multi-keV x-rays. Volumetric heating of low-density gas targets has been shown to be a very efficient method of producing x-rays.[5] However, gas targets are limited to a few photon energies (Ar K-shell: 3.1 keV, Kr L-shell: 1.8 keV, Xe L-shell: 4.5 keV, and Kr K-shell: 13.3 keV). For a given laser power, the efficiency also falls off sharply with increasing output x-ray energy.[6] X-ray-yield scaling in solid targets has been studied as a function of laser energy, laser wavelength, laser-pulse length and focusing properties.[7–13] Historically, solid targets, usually massive disks, have demonstrated efficiencies of only fractions of a percent for multi-keV photon energies. The efficiencies of these massive targets are compromised because much of the laser energy is deposited in a (relatively) low-density region at the critical surface, while the region of the target dominating the radiation output may be a higher-density region that must be conductively heated; steep gradients in solid targets make optimization of the multi-keV source difficult.[9] One hope to increase the efficiency of the solid targets is volumetrically to heat the whole target through a laser bleaching wave.[14]

Further author information: (Send correspondence to K.B.F.)
K.B.F.: E-mail: fournier2@llnl.gov, Telephone: 1 925 423 6129
M.C.M.: Permanent Address: Los Alamos National Laboratory, P.O. Box 1663 MS E540, Los Alamos, NM 87545

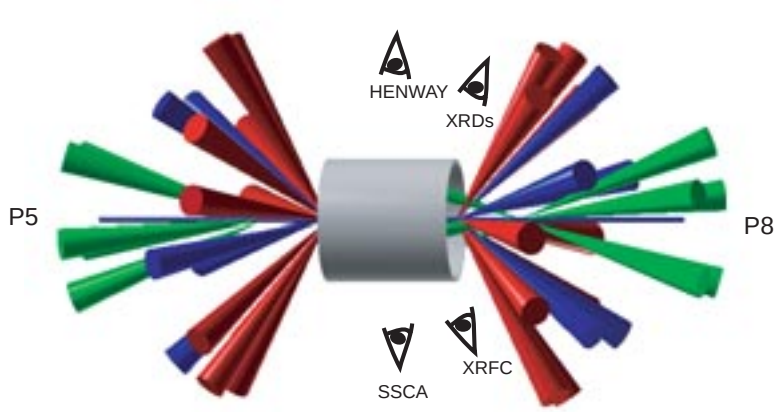

Figure 1. Schematic of our target, beam cones, and diagnostics used to measure the Ti x-ray output from the doped foam.

The current work presents measurements of x-ray output from laser-heated Ti K-shell emitters in a low-density aerogel plasma. We have achieved a density of $\rho = 3.1$ mg/cc in our aerogel targets, which gives an ionized density relative to the laser critical density of $0.09n_{\rm crit}$. Previous work with aerogel materials saw only subsonic heating at a density of $0.6n_{\rm crit}$.[15] Other works with low-density (organic) foams have ranged in density from $> 0.1n_{\rm crit}$ to $\sim 0.7n_{\rm crit}$,[15–18] and have all seen trans- or subsonic heating and large fractions of the incident energy scattered by parametric instabilities.[16,17] The targets of the present work show supersonic heating, x-ray output 1 – 3% of the incident laser energy, and minimal scattering losses.

2. EXPERIMENTAL SETUP

2.1. Foams

These experiments were carried out on the OMEGA laser at the Laboratory for Laser Energetics (LLE) at the University of Rochester. Four targets, at two different densities, were shot at two different laser intensities. The targets for these experiments were doped SiO_2 aerogels with an aggregate density of 3.1 or 3.3($\pm$ 0.1) mg/cc; the SiO_2 aerogel contained 3 atomic percent (atom%) Ti. Titanium and silicon alkoxides (monomers) were pre-mixed in an organic solvent to produce a homogeneous solution. The solution was poured into Be cylinders and co-polymerized to form a transparent, wet gel. The final aerogel material was formed by super-critical extraction of the solvent remaining in the wet-gel pores. The super-critical extraction for the solvent eliminates destructive compressive forces on the fragile gel network. This avoids a collapse of the sub-micron pore network of the gel, which would lead to densification. The density of the aerogel produced is determined by gravimetric analysis of the bulk sample. Analysis at an independent laboratory confirmed that the Ti remained at the 3 atom% level after the solvent-extraction process. Visual inspection confirmed that the Ti was uniformly dispersed throughout the sample (no optical scattering centers or crystallites). The cylindrical Be tubes had walls that were 80$\pm$5 μm thick. The walls had a transmission $\geq$ 90% for the Ti K-shell x-rays ($h\nu > 4.5$ keV) of interest. The cylinders were $\approx$ 2.2 mm long with a 2.0 mm inner diameter; these dimension are accurate to 3 – 5 μm. There was no detectable shrinkage of the aerogel material in the Be tube at the 3 atom% Ti level. These aerogel targets, when fully ionized, had an electron density that is 8.9 or 9.8×10^{20} cm^{-3} or 0.090 to 0.099 times the critical density, $n_{\rm crit}$, for 0.351 μm (3ω) light. This is, to the best of our knowledge, a record for the lowest density in an x-ray production experiment through laser heating of a large-volume solid target. A schematic of our target, laser-beam cones and the diagnostics used to measure the x-ray output from the target is shown in Fig. 1. The axis of the cylinder was along the P5-P8 OMEGA axis.

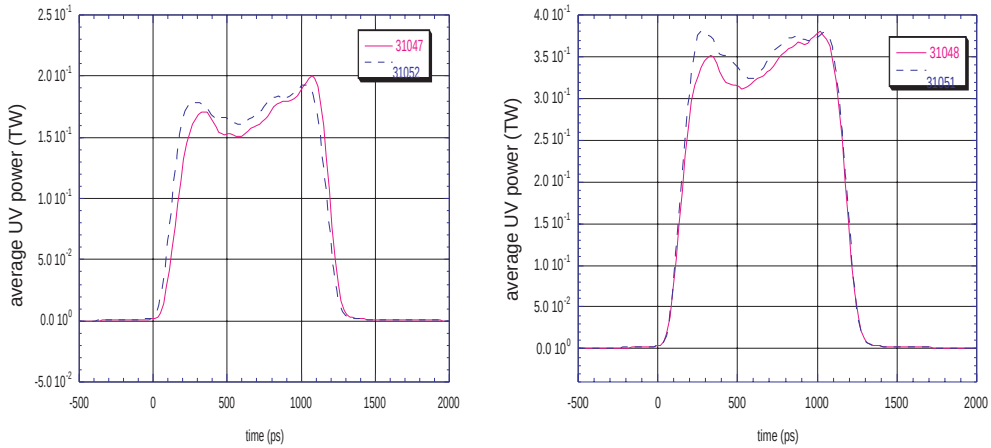

Figure 2. Average power (from 20 or 40 beams) delivered to one or both faces of our targets in these experiments.

Table 1. A summary of the shots in this series of experiments. Columns are OMEGA shot number, target density, laser intensity at the target face, total laser power and number of faces irradiated.

shot	ρ (mg/cc)	I_{Las} (10^{15} W/cm^2)	P_{Las} (TW)	Faces irradiated
31047	3.1	1.7	7.2	2
31048	3.1	3.3	14.5	2
31051	3.3	3.4	7.6	1
31052	3.3	1.7	3.8	1

2.2. Laser Pulses

Twenty beams were used in three cones on each face of the the target; two shots had both cylindrical faces irradiated, two shots had irradiation on a single face (see Table 1). Two cones with five beams each were at 21.4 and 42.0° to the target axis, the third cone, which had ten beams, was at 58.9° to the cylinder axis (henceforth, cone 1, 2 and 3, respectively). The 21.4° cone of beams was focused to 200 μm at a point 1100 μm from the face of the target, the other two cones are focused to 300 μm at the target's face. Differential polarization rotators (DPRs) were employed to smooth all beams. The DRPs increased the stated size of the focal spot for each cone by 70 μm. Beams in each cone had a footprint at the target face of $\approx$ 440, 475 and 650 μm, respectively. The experiment was designed to be fired with either 200 or 400 J per beam, for both cases of illumination to one or both faces, the measured average energies in each beam for each two-sided and each one-sided shot were, 180.7 362.6, 380.6 and 189.0 J/beam, respectively. One-ns-square pulses were used for irradiating the targets in these experiments. The laser-power profiles for our shots are shown in Fig. 2. The laser intensities in these experiments ranged from $I_{Las} = (1.7 - 3.4)\times10^{15}$ W/cm^2 at the target faces.

A summary of the four shots in this series is shown in Table 1. The dependence of our results on laser power, foam-target density and laser energy will be discussed below.

2.3. Diagnostics

Several diagnostics were used to measure the Ti K-shell output from these targets. The primary measurement was made with a two-channel crystal spectrometer[19] onto direct exposure film (DEF), both channels employed pertaerthritol (PET) crystals. The spectrometer looked at the wall of the target at an angle of 60° with respect to the cylinder axis. The known geometry of the spectrometer, crystal reflectivity (measured elsewhere[5]), the

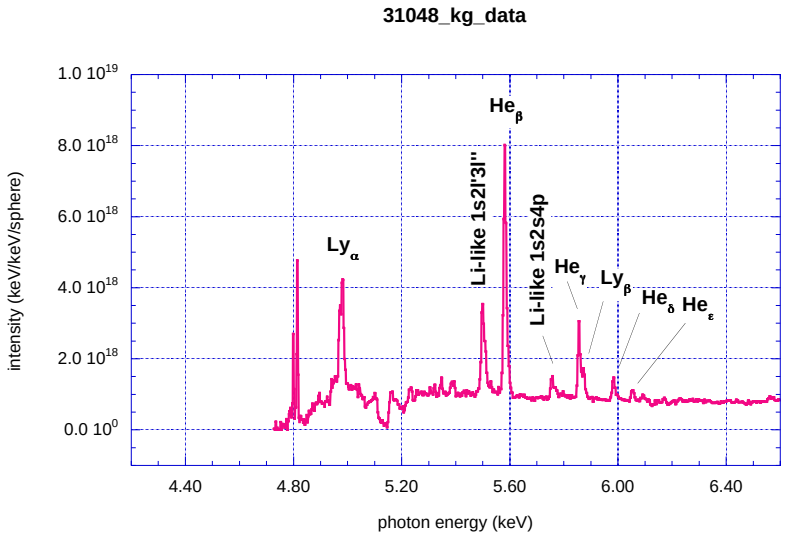

Figure 3. Ti K-shell spectrum, in absolute units, from the highest power shot (# 31048) in our series. The output integrated from 4.67 to 5.0 keV gives an output equal to 3.3% of the incident laser energy (14.5 kJ).

attenuation of the differential filters in front of the dispersive crystals, and the known response of the DEF[20] are used to compute the energy in a given spectral band. The films were digitized using a microdensitometer with a 22×22 μm^2 step size. The K-shell spectrum for Ti from the higher-energy channel is shown in Fig. 3. The signal in the H-like Ly$_\alpha$ line at 4.97 keV, as recorded on the higher-energy channel, and the signal in the He-like He$_\alpha$ ($1s2p \rightarrow 1s^2$, $h\nu = 4.75$ keV) band ($\Delta E = 0.11$ keV centered at 4.73 keV) found as described below are used to compute the performance of our targets. These spectral windows are similar to what has been reported in the literature for other Ti K-shell x-ray production experiments. Photometrically calibrated, filtered aluminum x-ray diodes were also fielded; they returned data on one shot (# 31052). The diode array viewed the target at the same angle with respect to the cylinder axis as the crystal spectrometer. The diode array has six independent channels filtered to cover the range from 1 to 10 keV. The deconvolved signal from the appropriate channels gives the total power radiated in a given spectral band (see Table 2 below).

Confirmation of supersonic heating[21] in these targets during the laser pulse is given by monitoring the position of the Ti x-ray front with a x-ray streak camera with a 20 μm wide slit oriented along the axis of the cylindrical target. The camera viewed the target at an angle of 79.2°. The streak camera was filtered with 20 μm of V and 5 mils Be, which gives a 10 – 20% transmission of the Ti K-shell x-rays. The slit is imaged on a 250 μm wide photocathode with a resulting magnification of 10×. The position of the x-ray emission front as a function of time is known to ≈ 0.11 mm. The raw streak data from the two 2-sided shots are shown in Fig. 4.

Two-dimensional images of the x-ray emission front in our target were obtained by a gated x-ray framing camera (XRFC). The XRFC was filtered with 16 mils of Be, which gave images of (essentially) pure Ti K-shell emission. The camera images were taken through 50 μm pinholes onto four strips of a MCP, each strip had three images taken approximately 200 ps apart and integrated for 80 ps. The camera had a view at a 63.4° angle with respect to the target axis. Two frames from shot 31048 (2-sided illumination, $P_{\rm Las} = 14.5$ TW, $I_{\rm L} = 3.3\times10^{15}$ W/cm^2) are shown in Fig. 5. The right edges of the pinholes in Fig. 5 seem to be slightly blocked. The XRFC data are consistent with the rates of axial propagation for the x-ray emission fronts found from the streak camera data, and showed only moderate curvature of the x-ray front as it moved down the tube. Additionally, six static x-ray pinhole cameras (XRPHC), at magnifications of 4× had views around the target at various angles. The view from the XRPHC, filtered with 6 mils of Be, at $\approx 72°$ with respect to the target axis is shown in Fig. 6. The outline of the Be cylinder is clearly visible, as are the footprints of the cone 3 beams. The emission is brightest from the center of the can, which is due to the peaking at late times of the target density after the two x-ray heat fronts have collided. This effect is also visible in the streaked images of Fig. 4.

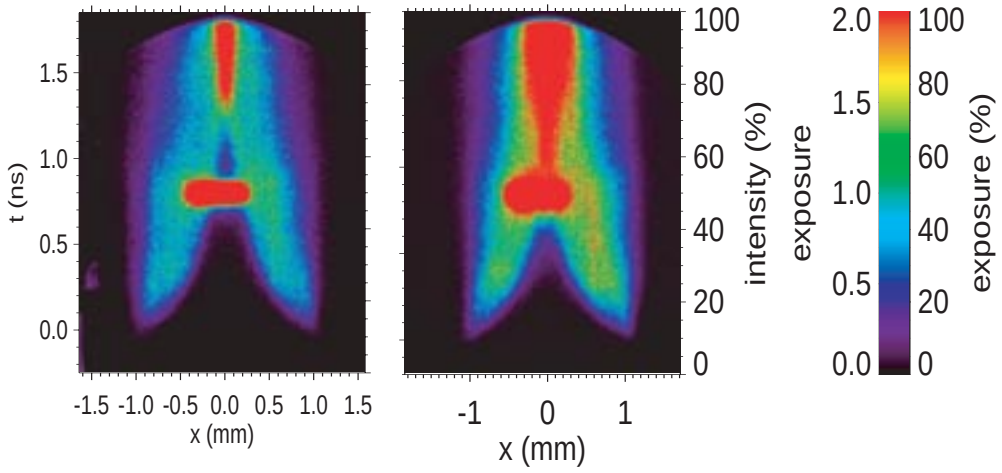

Figure 4. Streaked image of the propagation of Ti K-shell x-rays down the target axis. Time is in the vertical direction, and space is in the horizontal; the two faces of the target are at ± 1.1 mm. These data are for the two 2-sided illumination shots (# 31047 and 31048). The bright spot in the center of image is caused by straight through hard x-rays that burn the photocathode.

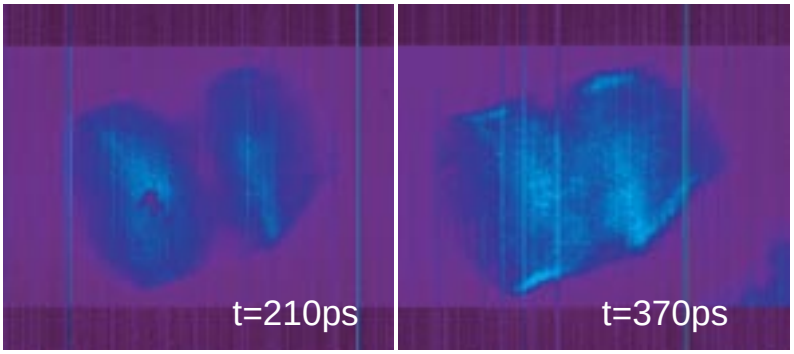

Figure 5. Two frames (t=210ps and 370ps) from # 31048 XRFC4 data (at 63.4° to the target axis) that clearly show the two lobes of plasma before they meet at the center of the cylinder.

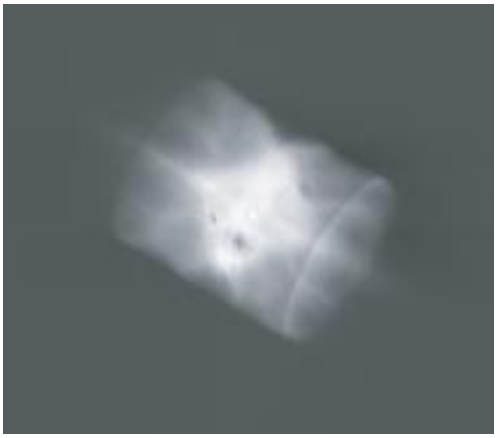

Figure 6. Time-integrated data from the XRPHC at $\theta = 79.3^\circ$, $\phi = 153.8^\circ$, at $\approx 72^\circ$ with respect to the target axis (shot # 31047).

Since we are interested in maximizing the output of our foam x-ray sources, we've measured the energy backscattered from the targets with LLE's full-aperture backscatter (FABS) system. Energy scattered from the target back into the optics of one cone 2 and one cone 3 beam was measured with both a calorimeter and spectrally with a streak camera. The streaked SRS channel showed spectrally narrow traces, centered at $2\lambda_0$ during the pulse duration, indicating a well defined quarter-critical surface in the target plasma. The streaked SBS data showed a signal broadened between 0.3 – 0.5 nm (FWHM), for low and high intensity shots, respectively, and centered ≈ 0.7 nm to the red of the laser wavelength. The SBS signal on the steeper cone 3 beam is consistently a factor of 2 – 5 larger than on the cone 2 beam, which may have to do with an interaction between the steeper cone 3 beam and the Be cylinder wall. The two measurements for the SRS data are within 15 – 20% of each other for all shots. The spectrally resolved scattering data are shown in Fig. 7. The calorimeter measured energy in the SRS and SBS channels is averaged over the two beam cones, then multiplied by 20 or 40 for one- or two-sided illumination to give the estimated total energy scattered from the target. Note, measured energy is only the energy scattered into the F/6.7 optic of the two beams used, and our analysis assumes that the scattering on the shallow-angle cone 1 beams is well described by the average of the measured scattering on the cone 2 and 3 beams. The result is that for the two low-power shots, the target scatters 2.3 – 4.0% of the incident energy, while for the two high-power shots, $\approx 5\%$ of the incident energy is scattered. We consider these levels to be negligible.

3. SIMULATIONS

We have used LASNEX,[22] a 2-D, Lagranian, radiation-hydrodynamics code to simulate these targets. The simulations have three cones of beams onto either one or two faces of the foam cylinder at angles of 21.4, 42.0 and 58.9 degrees with respect to the normal to the face. The focal spot is a super-Gaussian with 500 rays distributed across the spot's face. Ray-tracing techniques are used to model the laser propagation in the target, and inverse bremsstrahlung is the means by which laser energy is deposited. The simulations were run with the average experimental energy per beam, which ranged from 180.7 to 380.6 J/beam. In the simulation, the laser energy was delivered in a 1 ns square pulse with a 100 ps linear-ramp rise and fall. The resulting peak intensities in the simulations ranged from 1.8×10^{15} – 4.0×10^{15} W/cm^{-2}. Electron heat transport in the targets is described by a standard flux limited heat conduction model. We have varied the flux limiter in the simulations from 0.1 to 0.01, less inhibition to more, respectively. The best agreement with the measured heat-front position as a function of time is found for a flux limiter of 0.1 (see Section 4), although in the higher-intensity cases, no good agreement can be found in the simulation for anytime after ≈ 350 ps (similar to what Koch *et al.*[15] found for the

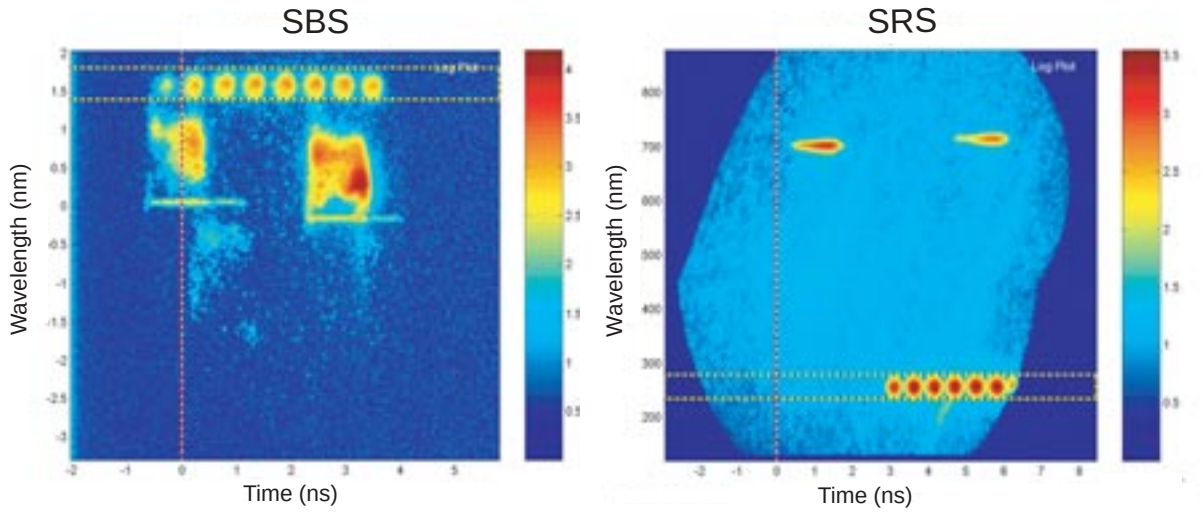

Figure 7. Shot # 31048 SBS (right panel) and SRS (left panel) streaked data. The signal from beam 25 (cone 2) is shown on the left of each panel, the signal from beam 30 (cone 3) is shown on the right of each panel. The SBS signal for beam 30 has been slightly offset below the reference wavelength.

same range of $I_{\rm Las}\lambda^2$). A finite-element treatment of both the electron heat conduction and radiation diffusion has been employed, this gives a more accurate solution to the conduction equations for distorted Lagrangian meshes.

Two atomic physics modules were used in LASNEX to compute the radiative emission from silicon, oxygen and titanium, they are XSN and DCA. XSN[23] is an average-atom atomic physics code that uses a simple Z-scaled, screened hydrogenic model to perform in-line calculations of arbitrary mixtures at all temperatures and densities. The lack of l-splitting and the simple line-width formulae limit the accuracy of the opacities to average values. Optical depths for the Ti K-shell lines emitted from our targets are far less than 1, and the system is optically thin to the Ti x-rays. The Detailed Configuration Accounting (DCA) atomic physics package[24] solves rate equations for the number of ions in each important excited state in each ionization state. This package is used when accurate atomic physics is needed for line diagnostics. DCA can handle any number of states connected by radiative and collisional bound-bound and bound-free, and auto-ionization and dielectronic recombination processes. The states and transition rates are specified in data files generated by other codes. Optionally, a simple screened hydrogenic model can be produced at problem initialization. This latter option was used in the present simulations. We find the DCA predictions to be $\approx 2\times$ larger than the XSN ones for the two higher-power shots.

4. RESULTS

Analysis of the propagation of laser heating in these targets has been discussed elsewhere.[21] Figure 8 shows the measured and predicted positions of the x-ray emission front for shot # 31052. The measured data are from the x-ray streak camera (data similar to Fig. 4), the simulation employs a flux-limiter of 0.1 and the DCA atomic physics package. The predicted x-ray emission front position is taken to be the coordinate of the most forward cell on axis in our simulation with an electron temperature $T_e > 1.7$ keV; the predicted position of the heat front starts to move backwards after 1 ns in the simulation because the laser pulse ends and the target starts to radiatively cool. We find initial velocities for the x-ray front moving down the target axis of 3 – 5 mm/ns for at least the first 200 ps, this is greater than $10\times$ the plasma's thermal-conduction sound speed. X-ray front velocities are still near 1 mm/ns at 300 ps. From the XRFC images, in the high-power 2-sided irradiation shot (# 31048, Fig. 5), we can see the x-ray emission fronts meeting at the target center by 600 ps after the start of

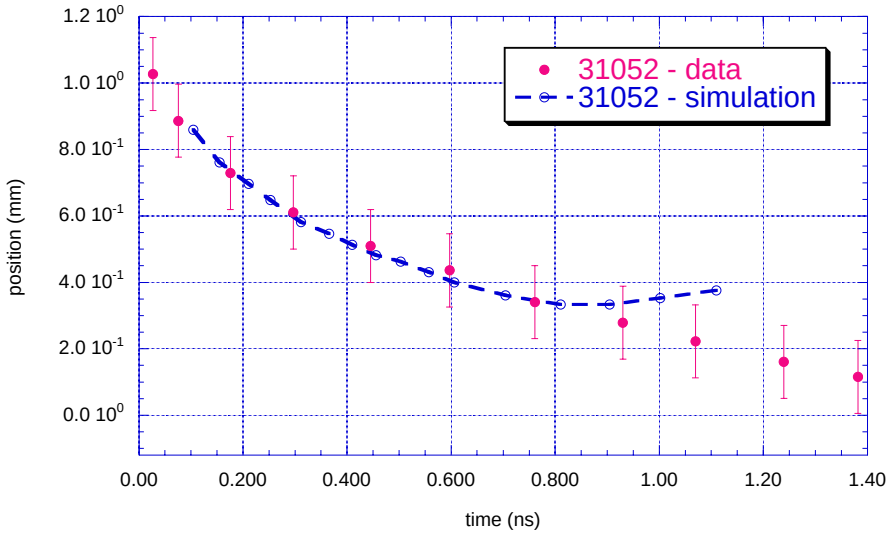

Figure 8. Measured and simulated x-ray emission front position as a function of time for shot # 31052 ($P_{\rm Las} = 3.8$ TW).

Table 2. Results for X-ray CE measurements: column are shot numbers, measured UV energy delivered to the target, the x-ray CE into $h\nu > 4.7$ keV from DEF, CE into $h\nu > 4.0$ keV from the XRDs, and the prediction from LASNEX.

shot	E_{UV} (kJ)	CE (%) DEF	CE (%) XRDs	CE (%) LASNEX
31047	7.2	1.8	–	0.53
31048	14.5	3.3	–	0.94
31051	7.6	1.6	–	1.01
31052	3.8	1.8	1.5	0.43

the pulse. From the measured positions of x-ray emission fronts[21] and the XRFC images, we demonstrate a fast, volumetric heating of the targets.

Table 2 summarizes our x-ray output measurements for our four shots. In the table are listed the measured conversion efficiency relative to the listed energy of each shot (2nd column) found by integrating the DEF (3rd column) from the H-like Ti^{21+} Ly_α transition at ≈ 4.9keV over a band 0.05 keV wide, and adding the contribution for the He_α line plus its associated satellites. The contribution from the He_α is found by calculating the ratio of He_α to Ly_α with a detailed collisional-radiative model.[25,26] The optical depths computed for the He_α line in these experiments are $\tau < 0.4$, so the comparison of lines strengths is not compromised by opacity effects. The whole series of He-like and H-like lines visible in Fig. 3 are fit with a single-temperature spectrum; the ratio of He_α to Ly_α from the model at that best-fit temperature is then used to compute the contribution of He_α to the total Ti K-shell signal. The relative strength of He_α to Ly_α is then checked for consistency with the Ti spectrum measured in the lower-energy channel of the spectrometer. Shots 31047 and 31052 were fit very well for $T_e = 2.0$ keV ($He_\alpha/Ly_\alpha = 19.8$), while shots 31048 and 31051 were fit at $T_e = 2.25$ keV ($He_\alpha/Ly_\alpha = 12.6$). The ratios of He_α to Ly_α observed in the lower-energy channel are within $\approx 40\%$ of these numbers. There is an overall $\pm$ 30% uncertainty on the CE numbers measured with the DEF that results from measured uncertainties in crystal reflectivity across the width of the crystal,[5] relative transmissivity of differential filters, and the level of film background. The signal measured with the XRDs in the band from 4 to 6 keV for shot 31052 is also listed, there is a $\pm$ 20% error bar on the deconvolved XRD signal. The XRD signal contains the contribution from the higher-n members of the He- and H-like Rydberg series, aside from He_β, their contributions are negligible. The targets in shots 31047 and 31048 had densities that were $\approx 6\%$ lower than those in 31051 and 31052, the data

in Table 2 do not let us assess if this difference in density (0.090 versus $0.099 n_{\rm crit}$) is meaningful. The measured CE for shots 31047 and 31051 were $\approx 1/2$ that of # 31048, this scales directly with the total energy delivered to the target. However, there is not a drop in CE for # 31052, which had $\approx 50\%$ of the energy of 31047 and 31051. The laser intensity on each face of the target was a factor of two greater in # 31051 than # 31047 (3.4×10^{15} versus 1.7×10^{15} W/cm^2), the resulting CEs seem independent of intensity in this case.

Also listed in Table 2 is the prediction for the x-rays out from our targets from a two-dimensional radiation-hydrodynamic simulation (Section 3); the Ti spectrum in the simulation is integrated from 4.4 keV up to 5.1 keV, thus including the $\rm He_\alpha$ and $\rm Ly_\alpha$ lines. The CE numbers from the DCA runs for each OMEGA shot are listed in the last column of Table 2, which are generally larger than the predicted CEs using the XSN package in LASNEX (see Section 3). In every case, the targets appear to perform better than predicted by the simulations. As stated in § 2.3, the measured scattering energy losses from the targets are less than 5%. If the incident energies in Table 2 are reduced by this amount, the measured CEs are increased by $\approx 0.1\%$, a negligible amount.

5. SUMMARY AND DISCUSSION

We have demonstrated supersonic heating of large, low-density Ti-doped aerogel targets.[21] Our targets contained 3 atom% Ti in $\rm SiO_2$ aerogel, which when full ionized had electron densities in the range $0.09 - 0.1 n_{\rm crit}$. Ti K-shell x-rays are measured with a x-ray crystal spectrometer and, for one shot, calibrated x-ray diodes. Output in the 4.67 – 5.0 keV band from 1.6 – 3.3% of the incident laser energy is observed with the spectrometer, output of 1.5% is measured in the 4 – 6 keV band with the diodes. The supersonic heating by the laser-drive beams is complimented in our low-density targets by low levels of laser-scattering energy losses.

Large x-ray sources are necessary for backlighters for flash radiograph of large targets; the x-ray source must be larger than the object being imaged. The requirement for a large source brings with it the requirement for a large amount of energy to heat the whole volume. If heating takes place by (slow) thermal conduction, the possibility for heating large volumes, and for good time resolution, is seriously compromised. The present work looks at laser heating of low-density foams doped with a multi-keV emitter (K-shell Ti at 4.5 keV). The targets demonstrate super-sonic heating by a laser-bleaching wave, thus suggesting that large-scale, efficient volumetric heating takes place. If the target has a high enough absolute brightness, then a point backlighter can be created using a pinhole. The way to maximize the absolute brightness of these foams is to increase the Ti-doping level. Doubling the doping fraction doubles the number of emitters, and hence, our design calculations show that doubles the target output. This is because our targets are still optically thin for the Ti K-shell radiation, and the assumed low-density means the whole volume of the target is quickly heated. At the present time, we have not determined the appropriate conditions to prepare a 6 atom% Ti-doped silica aerogel that exhibits minimal shrinkage (collapse), at a density ≤ 3 mg/cc. This may be primarily due to the different rates of polymerization of the two species. This rate consideration is even more pertinent if we hope to move to a higher-Z (heavier) dopant, such as Zn, which has a strong K-shell output in lines around 9.0 keV. Initial experiments, however, have shown promise for incorporating Zn in a 3 mg/cc silica matrix at the 3 atom% level. Strong K-shell emission from higher-Z materials is definitely possible given the increasing energy of current laser systems (such as the NIF). Assuming the targets with higher levels of doping do not suffer from shrinking or pinching in the molds, and that the chemistry can be worked out so that the aerogel material and the impurity gel at the same rate, doped foams seem like a promising avenue for bright x-ray source development.

Finally, we note that previous work has found CEs for Ti targets that ranged from 0.01 – 0.6%[7, 8, 10, 11] for lasers at 2ω and 3ω (0.53 and 0.35 μm) with pulse lengths 100 – 500 ps. The targets of the present work were irradiated with ns-scale pulses, these targets performed between a factor of 3 – 5 better than the results reported by Yaakobi *et al.*,[7] which are the highest published CEs for Ti that we have found. The improvement in performance for our targets compared to those in in Yaakobi *et al.* scales nearly linearly with the increase of laser intensity in these experiments above that in Yaakobi *et al.* Much work remains to be done developing and optimizing the low-density, doped-foam targets as bright, efficient x-ray sources.

ACKNOWLEDGMENTS

This work was performed under the auspices of the U.S. Department of Energy by University of California Lawrence Livermore National Laboratory under contract No. W-7405-Eng-48.

REFERENCES

1. N. C. Woolsey, D. Riley, and E. Nardi, "Kilovolt x-ray scattering from a plasma," *Rev. Sci. Instru.* **69**, pp. 418–424, 1998.
2. F. Ze, D. R. Kania, S. H. Langer, H. Kornblum, R. Kauffman, J. Kilkenny, E. M. Campbell, and G. Tietbohl, "Observation of enhanced x-ray emissoin from long-pulse-width laser-produced plasmas," *J. Appl. Phys.* **66**, pp. 1935–1939, 1989.
3. S. G. Glendinning, J. Colvin, S. Haan, D. H. Kalantar, O. L. Landen, M. M. Marinak, B. A. Remington, R. Wallace, C. Cherfils, N. Dague, L. Divol, D. Galmiche, and A. L. Richard, "Ablation front Rayleigh-Taylor growth experiments in spherically convergent geometry," *Phys. Plasmas* **7**, p. 2033, 2000.
4. S. R. Goldman, S. E. Caldwell, M. D. Wilke, D. C. Wilson, C. W. Barnes, W. W. Hsing, N. D. Delamater, G. T. Schappert, J. W. Grove, E. L. Lindman, J. M. Wallace, R. P. Weaver, A. M. Dunne, M. J. Edwards, P. Graham, and B. R. Thomas, "Shock structuring due to fabrication joints in targets," *Phys. Plasmas* **6**, p. 3327, 1999.
5. C. A. Back, J. Grun, C. Decker, L. J. Suter, J. Davis, O. L. Landen, R. Wallace, W. W. Hsing, J. M. Laming, U. Feldman, M. C. Miller, and C. Wuest, "Efficient multi-kev underdense laser-produced plasma radiators," *Phys. Rev. Lett.* **87**, p. 275003, 2001.
6. R. Kauffman, "X-ray radiation from Laser Plasma," in *Handbook of Plasma Physics*, A. M. Rubenchik and S. Witkowski, eds., **vol. 3**, pp. 111–162, Elsevier, Amsterdam, 1991.
7. B. Yaakobi, P. Bourke, Y. Conturie, J. Delettrez, J. M. Forsyth, R. D. Frankel, L. M. Godman, R. L. McCrory, W. Seka, J. M. Soures, A. J. Burek, and R. E. Deslattes, "High x-ray conversion efficiency with target irradiation by a frequency tripled nd-glass laser," *Opt. Commun.* **38**, pp. 196–200, 1981.
8. D. L. Matthews, E. M. Campbell, N. M. Ceglio, G. Hermes, R. Kauffman, L. Koppel, R. Lee, K. Manes, V. Rupert, V. W. Slivinsky, R. Turner, and F. Ze, "Characterization of laser-produced plasma x-ray sources for use in x-ray radiography," *J. Appl. Phys.* **54**, pp. 4260–4268, 1983.
9. R. Kodama, K. Okada, N. Ikeda, M. Mineo, K. A. Tanaka, T. Mochizuki, and C. Yamanaka, "Soft-x-ray emission from ω_0, $2\omega_0$, and $4\omega_0$ laser-produced plasmas," *J. Appl. Phys.* **59**, pp. 3050–3052, 1986.
10. D. Phillion and C. J. Hailey, "Brightness and duration of x-ray-line sources irradiated with intense 0.53μm laser-light at 60 and 120 ps pulse width," *Phys. Rev. A* **34**, pp. 4886–4896, 1986.
11. G. J. Tallents, M. H. Key, A. Ridgeley, W. Shaikh, C. L. S. Lewis, D. O'Neill, S. J. Davidson, N. J. Freeman, and D. Perkins, "An investigation of the x-ray point-source brightness for a short-pulse laser plasma," *J. Quant. Spectrosc. Radiat. Transf.* **43**, pp. 53–60, 1990.
12. G. A. Kyrala, R. D. Fulton, E. K. Wahlin, L. A. Jones, G. T. Schappert, J. A. Cobble, and A. J. Taylor, "X-ray generation by high irradiance subpicosecond lasers," *Appl. Phys. Lett.* **60**, pp. 2195–2197, 1992.
13. J. Workman and G. A. Kyrala, "X-ray yield scaling studies performed on the OMEGA laser," *Rev. Sci. Instru.* **72**, pp. 678–681, 2001.
14. J. Denavit and D. W. Phillion, "Laser ionizatoin and heating of gas targets for long-scale-length instability experiments," *Phys. Plasmas* **1**, pp. 1971–1984, 1994.
15. J. A. Koch, K. G. Estabrook, J. D. Bauer, C. A. Back, L. Klein, A. M. Rubenchik, E. J. Hsieh, R. C. Cook, B. J. MacGowan, J. D. Moody, J. C. Moreno, D. Kalantar, and R. W. Lee, "Time-resolved x-ray imaging of high-power laser-irradiated underdense silica aerogel and agar foams," *Phys. Plasmas* **2**, pp. 3820–3831, 1995.
16. K. A. Tanaka, B. Boswell, R. S. Craxton, L. M. Goldman, F. Guglielmi, W. Seka, R. W. Short, and J. M. Soures, "Brillioun scattering, two-plasmon decay, and self-focusing in underdense ultraviolet laser-produced plasmas," *Phys. Fluids* **28**, pp. 2910–2914, 1985.
17. H. Figueroa, C. Joshi, and C. E. Clayton, "Experimental studies of Raman scattering from foam targets using a 0.35 μm laser beam," *Phys. Fluids* **30**, pp. 586–592, 1987.
18. V. V. Gavrilov, A. Y. Gol'tsov, N. G. Koval'skii, S. N. Koptyaev, A. I. Magunov, T. A. Pikuz, I. Y. skobelev, and A. Y. Faenov, "X-ray spectral measurements of high-temperature plasma parameters in porous targets irradiated with high-power laser pulses," *Quantum Electronics* **31**, pp. 1071–1074, 2001.
19. L. N. Koppel and J. D. Eckels, Lawrence Livermore National Laboratory Report, UCRL-79781, 1977.

20. B. L. Henke, J. Y. Uejio, G. F. Stone, C. H. Dittmore, and F. G. Fujiwara, "High-energy x-ray response of photographic films - models and measurement," *J. Opt. Soc. Am. B* **3**, p. 1540, 1986.
21. C. Constantin *et al.*, "Experimental investigations of supersonic radiation heat wave propagation in laser-produced under-dense plasmas," *Phys. Rev. Lett.*, submitted summer, 2003.
22. G. Zimmerman and W. Kruer, "Numerical simulation of laser-initiated fusion," *Comments Plasma Phys. Control. Fusion* **2**, pp. 51–61, 1975.
23. W. A. Lokke and W. Grasberger, "XSNQ-U: A non-LTE emission and absorption coefficient subroutine," Lawrence Livermore National Laboratory Report, UCRL-52276 , 1977.
24. Y. T. Lee, "A model for ionization balance and L-shell spectroscopy of non-LTE plasmas," *J. Quant. Spectrosc. Radiat. Transf.* **38**, pp. 131–145, 1987.
25. S. H. Glenzer, K. B. Fournier, C. Decker, B. A. Hammel, R. W. Lee, L.Lours, B. J. MacGowan, and A. L. Osterheld, "Accuracy of K-shell spectra modeling in high-density plasmas," *Phys. Rev. E* **62**, pp. 2728–2738, 2000.
26. C. Biedermann, R. Radtke, and K. B. Fournier, "Spectroscopy of heliumlike argon resonance and satellite lines for plasma temperature diagnostics," *Phys. Rev. E* **66**, p. 066404, 2002.